New Results on Nuclear Fission – Data and Interpretation

Aleksandra Kelić, Maria Valentina Ricciardi, and Karl-Heinz Schmidt

Gesellschaft für Schwerionenforschung G.m.b.H.,(GSI), Planckstr. 1, 64291 Darmstadt, Germany

Abstract. An overview on phenomena observed in low-energy fission is presented, including new results from a GSI experiment with relativistic secondary beams. The interpretation of the structural effects in terms of fission channels reveals an astonishing stability of the fission-channel positions in the heavy fragment in nuclear charge in contrast to the previously assumed constancy in mass. The statistical model is applied to deduce the relevant characteristics of the potential-energy surface. It is assumed that the different degrees of freedom are frozen at a specific stage each on the descent from saddle to scission due to the fission dynamics. Evidence for the separability of compound-nucleus and fragment properties in fission is deduced.

Keywords: Nuclear fission, Radioactive beams, Fission channels, Influence of fragment shells.
PACS: 24.75.+i, 25.85.-w, 25.85.Jg, 27.80.+w, 27.90.+b, 29.38.Db, 24.10.Pa

INTRODUCTION

The energy-dependent fission cross sections and the properties of fission fragments, like their yields as a function of mass and nuclear charge, their kinetic energies and the number and the energies of emitted neutrons and gamma rays, show very complex features in low-energy fission, which may strongly differ from one fissioning system to another. While the explicit prediction of the resonance behavior of the fission cross section seems to be impossible, several attempts have been made to develop theoretical models for calculating the properties of the fission fragments and their subsequent decay. Most elaborate models are based either on the macro-microscopic approach, e.g. [1,2], or they have been developed on a microscopic basis [3]. Still, the realistic modelling of fission, as a prominent example of an out-of-equilibrium process, represents a severe challenge.

From the experimental side, one of the problems encountered in this field is the rather limited number of systems investigated. This contribution concentrates on an empirical overview upon features of nuclear structure in the fission-fragment properties in low-energy fission and on deducing some common features behind the large variety of the complex observations made for the different fissioning systems. Recent results from experiments with relativistic secondary beams performed at GSI, Darmstadt, have increased our empirical knowledge considerably and play a key role in this context.

Besides its importance for fundamental research, a better quantitative understanding of fission is required by its applications in other fields. Nuclide production yields determine the amount and the time distribution of delayed neutrons, which are important for the operation of fission reactors [4] and for detecting fissile material [5]. They are also important for the perspectives for the production of very neutron-rich isotopes in secondary-beam facilities, e.g. [6,7]. The nuclide production in the fission of extremely neutron-rich nuclei on the astrophysical r-process path is a particularly challenging problem [8].

EMPIRICAL KNOWLEDGE

The present empirical knowledge on nuclear structure in fission-fragment yields is illustrated in Figure 1. The figure shows mass distributions from particle-induced fission of stable or long-lived fissile targets, spontaneous fission of nuclei produced by heavy-ion fusion or breading, and element distributions from the electromagnetic–induced fission of secondary projectiles.

The latter, which cover the largest contiguous field of fissioning systems on the chart of the nuclides, stem from one experiment performed in inverse kinematics at GSI, Darmstadt [9]. This experiment exploits a new technique to investigate low-energy fission. Relativistic secondary projectiles are produced via fragmentation of a 1 *A* GeV primary beam of ^{238}U and identified in nuclear mass and charge number by the fragment separator FRS. In a dedicated experimental set-up, the

giant resonances, mostly the giant dipole resonance, are excited by electromagnetic interactions in a secondary lead target, and fission from excitation energies around 11 MeV is induced. Both fission fragments are identified in nuclear charge, and their velocity vectors are determined. From these data, the element yields and the total kinetic energies are deduced.

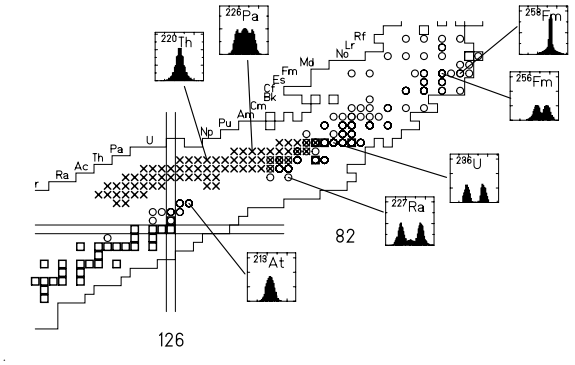

FIGURE 1. Systematic overview on the structural features in the mass, respectively nuclear-charge distributions of fission fragments. Systems investigated in the GSI experiment [9] are marked by crosses, those measured by other approaches are shown by open points. See ref. [9] for original references. The insets show the mass, respectively element distributions of the fission fragments for a few selected systems.

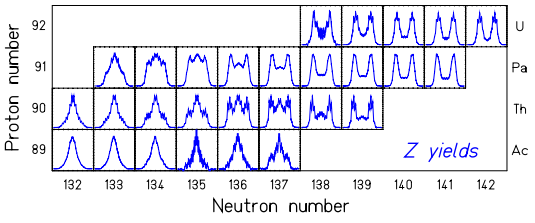

FIGURE 2. View on nuclear-charge distributions of fission fragments drawn on the position of the fissioning system on the chart of the nuclides. These systems were investigated in the GSI experiment [9]. (Figure is taken from ref. [10].)

The distributions shown in Figures 1 and 2 can roughly be classified as a function of the mass of the fissioning system: There is a gradual transition from a single Gaussian to a double-humped distribution around A=226, with triple-humped distributions appearing in the transition region. Above A=257, the distribution changes abruptly to a narrow symmetric one. Strong signatures of nuclear structure are also found in the total kinetic energy (TKE), the mass-dependent neutron-emission yields and other observables.

PROPERTIES OF FISSION CHANNELS

It has been proposed to interpret the combined signatures of nuclear structure in fragment yields and TKE as the manifestation of independent fission channels. The flux in the descent from saddle to scission is assumed to follow specific valleys in the potential-energy surface in direction of elongation [11,12]. The fission channels are characterized by several parameters, e.g. the average mass or charge split, the mass or charge width, and the mean total kinetic energy, respectively the elongation of the scission configuration.

As examples, Figure 3 shows the measured element-yield distributions and the mean total kinetic energies for the systems ^{233}U, ^{232}Pa, ^{228}Pa, ^{228}Th, ^{226}Th, and ^{223}Th, which were determined in the GSI experiment [9]. In a simultaneous fit to elemental yields and total kinetic energies, it was possible to reproduce these data with the assumption of independent fission channels.

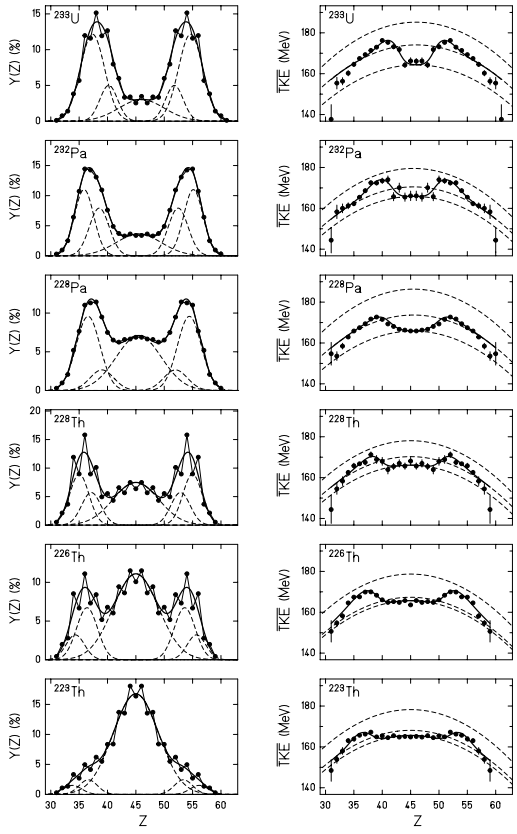

FIGURE 3. Data points: Measured elemental yields (left column) and mean total kinetic energies (right column) for six selected systems. Full lines: Description with independent fission channels. Dashed lines: Individual contributions of super long, standard I, and standard II fission channels. (Figure is taken from ref. [10].)

A satisfactory description of the data was obtained with three channels, "standard I", close to N=82, "standard II" around N=88, both in the heavy fragment, and "super long" at symmetry, following the notation introduced by Brosa et al. [12]. Each channel was represented by a Gaussian distribution in the yields and a specific elongation of the scission-point configuration. In order to consider the trivial variation of the total kinetic energy as a function of mass and charge split, the Coulomb repulsion V_C in the scission-point configuration was parameterized by the following expression, introduced in ref. [13]:

$$V_C = \frac{Z_1 \cdot Z_2 \cdot e^2}{r_0\left(A_1^{1/3} \cdot \left[1+\frac{2\beta_1}{3}\right] + A_2^{1/3} \cdot \left[1+\frac{2\beta_2}{3}\right]\right) + d} \qquad (1)$$

Z_i, A_i, and β_i are nuclear-charge numbers, mass numbers and quadrupole deformations of the fission fragments, d is the tip distance at scission, r_0=1.16 fm is the nuclear-radius constant, and e is the elementary charge. Although all three parameters β_1, β_2 and d are expected to vary from one fission channel to another, the deformation parameters β_i=0.6 were kept constant, and only d was adjusted to the data.

The parameters of the independent fission channels were compared for the whole body of available data. A compilation of these data and the original references can be found in ref. [14]. The data are restricted to spontaneous fission and to initial excitation energies up to a few MeV above the fission barrier, where structural effects are expected to be strong.

The standard deviation of the standard I (standard II) fission channel amounts to about 3.5 (5) mass units. The width of the super-long fission channel is well determined for the lightest systems to about 10 mass units, while the extracted values fluctuate strongly for heavier system, probably reflecting the large uncertainty due its tiny yield.

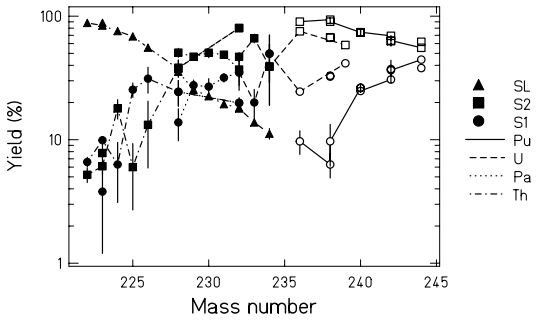

FIGURE 4. Relative yields of the fission channels (super long, standard I and standard II) as a function of the mass number of the fissioning system. Data of ref. [9] are marked by full symbols, data from other sources by open symbols.

Figure 4 shows the relative yields of the different fission channels. There is a clear tendency: The relative yield of the symmetric super-long fission channel shows an exponential decrease with increasing mass number, while the complementary yield of the lumped asymmetric component increases accordingly.

The systematic trend in the competition between the standard I and the standard II channels can best be derived from the data of protactinium and plutonium isotopes, which have the smallest uncertainties. These two elements show a consistent trend: The relative weight of the standard I fission channel grows strongly with increasing neutron excess, when the nuclides produced in the standard I fission channel move closer to the doubly magic ^{132}Sn on the chart of the nuclides.

Another salient feature of the standard I and standard II fission channels is depicted in Figure 5: The mean positions of the heavy components turn out to be remarkably stable in atomic number, while they move considerably in neutron number and consequently also in mass number. This finding sheds new light on the well known observation of Unik et al. [15], who stated that the position of the heavy component of the fission-fragment distributions in asymmetric fission is approximately constant in mass over the whole range of fissioning systems investigated. On the basis of Figure 5 we re-formulate more precisely: It is not the mass number but *the element number*, which *is primarily kept constant*.

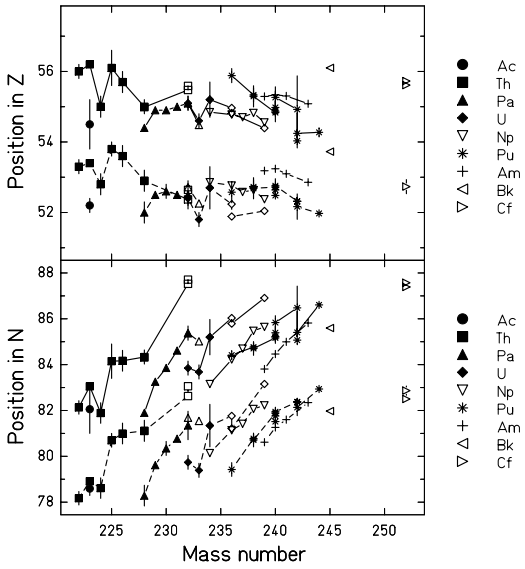

FIGURE 5. Mean positions of the standard fission channels in atomic number (upper part) and neutron number (lower part) for different isotopic chains. The points of standard I (standard II) are connected by dashed (full) lines. Data of ref. [9] are marked by full symbols. Conversion between A, Z, and N has been performed using the UCD assumption, neglecting neutron evaporation.

THE SEPARABILITY PRINCIPLE

Since theoretical models reproduce the measured properties of the fission fragments only with a rather limited precision, empirical systematics are still needed for technical applications. However, due to the complex variations of the observed phenomena as a function of the composition of the fissioning system, they are not suited for accurate predictions for systems which are not accessible to experiment. In the present chapter, we would like to propose a new kind of empirical description of the fission process, which reveals some global tendencies and ordering principles behind the complex observations and which has the capability for robust extrapolations.

We take the statistical model as the basis of our considerations. However, its application to an out-of-equilibrium process is not straightforward. Scission-point models (e.g. [13]) are in conflict with many observations: E.g. in light-particle-induced fission the distribution of K quantum number, which is the projection of the angular momentum on the symmetry axis, is well described by the statistical model when applied at saddle [16,17]. In general, it is the time scale of the process that is responsible for the evolution of a specific degree of freedom in comparison to the dynamical time of the fission process, which determines the configuration that is most relevant for a specific observable, e.g. [18,19].

Applying the statistical model to a specific configuration on the fission path offers the possibility to deduce the relevant properties of the potential-energy surface from experimental data. This approach has been applied in refs. [20,21,22] to deduce the mass-asymmetric potential from measured mass distributions. At high excitation energies, when shell effects have washed out, this procedure yields the stiffness of the macroscopic potential. By analyzing the body of available data, the authors of refs. [20,22] established a global parameterization as a function of the fissility of the system.

Applying the same approach to fission-fragment mass distributions measured at lower excitation energies, the microscopic correction to the potential energy has been extracted [21]. We extend this procedure by applying it to a much larger range of fissioning systems and by considering the microscopic correction in neutron and proton number, and not in mass number as done in ref [21]. Figure 6 shows the results for ^{226}Th, ^{239}U, ^{252}Cf, and ^{260}Md. (See ref. [23] for references of the original data.) The microscopic corrections in the configuration, which is relevant for the mass split, were deduced by assuming a constant-temperature level density above the barrier and the Hill-Wheeler approach below the barrier. The parameter values applied are listed in Table 1. For spontaneous fission, the oscillator energy of the inverted parabola of the outer barrier is given by $\hbar\omega = 2\pi \cdot T_{eff}$.

TABLE 1. Parameters used for Figure 6.

System	σ_A (macroscopic)	T_{eff}
^{226}Th ($E^*\approx$11 MeV)	8.8	0.6 MeV
^{238}U(n,f), E_n=1.7 MeV)	9.5	0.4 MeV
^{252}Cf (spont. fission)	11.3	0.6 MeV
^{260}Md (spont. fission)	12.2	0.6 MeV

Two-centre shell-model calculations, e.g. [24], suggest that the microscopic corrections to the potential energy beyond the outer saddle are strongly influenced by the shells of the separated fragments. This leads us to the following conclusion: While the macroscopic potential can be parameterized as a function of Z^2/A of the compound nucleus, the microscopic potential is determined by the numbers of neutrons and protons in the nascent fragments. This *separability principle of compound-nucleus and fragment properties* on the fission path represents a powerful ordering scheme. It suggests that the microscopic structures deduced in Figure 2 can be traced back to shells in the fragments, which should be the same for all systems.

The success of this approach is illustrated in Figure 7 in a schematic way. Obviously, the complex behavior of microscopic structure as a function of mass asymmetry of the four systems shown in Figure 6 can be reproduced already rather well as a superposition of only two shells at N=82 and N=92. The choice of these shells is motivated by shell-model calculations [13,25]. As a specific feature, in ^{260}Md the N=82 shell is approximately met in both fragments at the same time. This overlay is the reason for the strong and narrow shell effect at symmetry, which leads to the appearance of the narrow symmetric fission component observed in this system.

The parameters of the shells used in Figure 7 are listed in Table 2. Following the results of theoretical calculations of ref. [26], we consider for ^{226}Th, ^{239}U, and ^{252}Cf, where in the standard I fission channel the spherical heavy fragment is formed together with a strongly deformed light fragment, that the N=82 shell appears at N=85 in the final fragments, assuming that the heavy fragment receives three neutrons from the neck.

TABLE 2. Shell parameters.

Shell	Depth	Width (σ_A)
N=82	-3.3 MeV	3.5
N=92	-4.0 MeV	7.0

A more realistic description should include the influence of additional shells. E.g. the Z=50 shell would be needed to explain the strong charge polarization of the standard I fission channel, where the heavy fragments tend to approach the doubly-magic ^{132}Sn.

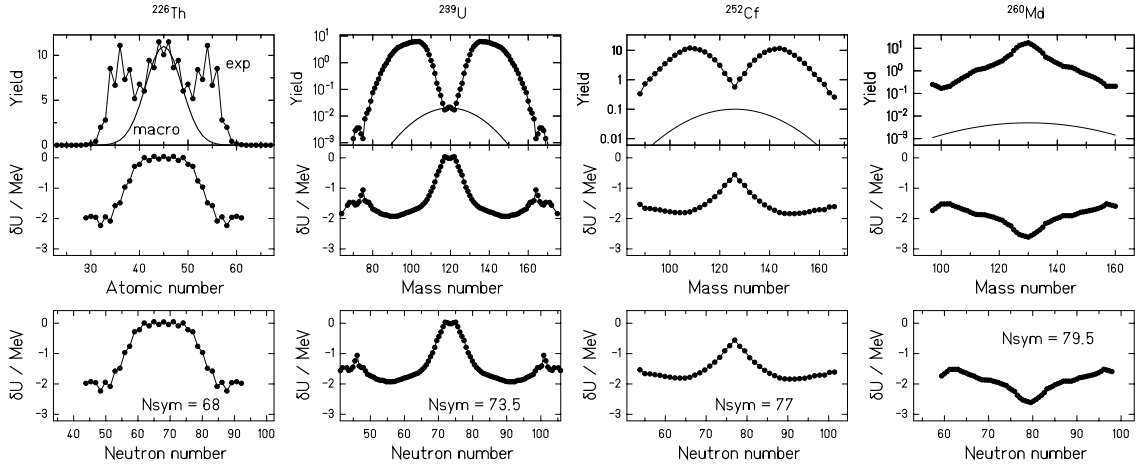

FIGURE 6. Extraction of the microscopic potential responsible for the nuclear-charge or mass split in fission. The amount the measured yields (data points in the upper row) exceed the macroscopic prediction (smooth lines) is attributed to the microscopic energy at saddle. The microscopic energies are displayed as a function of atomic number and mass number, respectively, (second row) and in a projection on neutron number (third row).

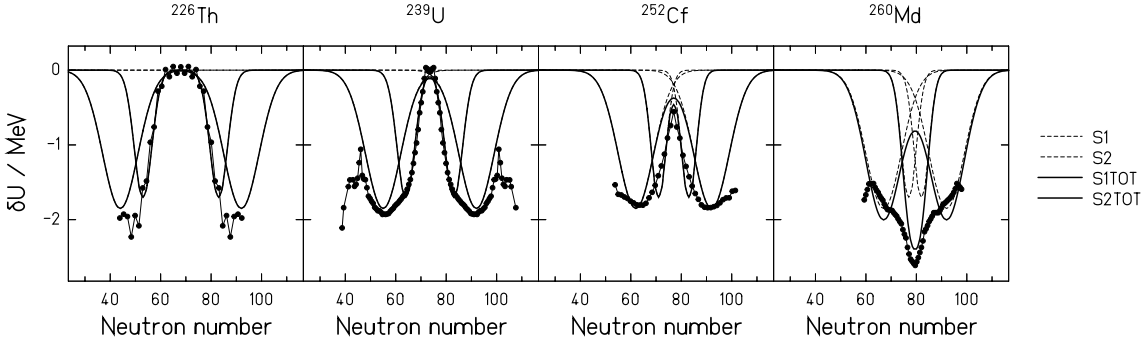

FIGURE 7. Comparison of the empirical microscopic potential (points) and two adopted neutron shells (lines) at N=82 (standard I) and N=92 (standard II). For ^{252}Cf and, more strongly for ^{260}Md, the same shells overlap in the two fragments, and thus their sums (SITOT, S2TOT) form the corresponding fission valleys. Data points at very large mass asymmetry, which are assumed to be uncertain, are marked be open symbols.

The separability principle makes our approach technically rather similar to the scission-point model of Wilkins et al. [13]. In both cases, the yields of the fission fragments are determined by the phase space above the mass-asymmetry dependent potential. There is, however, an important difference; While Wilkins et al. considered the potential energy at the scission point to govern the nuclide formation in fission, the present approach assumes that the potential in a configuration somewhere between saddle and scission is decisive for the mass split in fission. In this way the time scale of the fission process is taken into account. Only due to the application of the separability principle we assume that the shell effects of the fragments are decisive already at an earlier stage on the fission path.

CONCLUSION

A systematic overview on the experimental knowledge in low-energy fission was presented. The data could well be parameterized by means of the model of independent fission channels with adjusted parameters.

The parameters of the fission channels vary in a smooth and systematic way between actinium and californium. As the most remarkable results, the positions of the heavy components of the asymmetric fission channels were found to be stable in atomic number, while they move strongly in mass as well as in neutron number. Finally, the microscopic features of the mass-dependent fission yields could be traced back to shells in the nascent fragments. The separability of compound-nucleus and fragment properties of the system on the fission path seems to be realized to a good approximation and makes the macro-microscopic approach particularly strong in its application to nuclear fission. By deducing the microscopic corrections to the potential energy from the measured fission-fragment nuclide yields and attributing those to two major shells in the nascent fragments, we arrived at a remarkably realistic reproduction of the microscopic features of fission over the whole range covered by experiment.

ACKNOWLEDGMENTS

This work has been supported by the GSI Hochschulprogramm and by the Bundesministerium für Bildung, Wissenschaft, Foschung und Technologie under Contract number BMBF 06 DA 473. Further support came from the European Union under the contracts FIKW-CT-2000-031 (HINDAS), FI6W-516520 (EUROTRANS), HPRI-1999-CT-50001 (EURISOL_RD), and RIDS 515768 (EURISOL_DS).

REFERENCES

1. T. Asano, T. Wada, M. Ohta, S. Yamaji, H. Nakahara, *J. Nucl. Radioch. Sc.* **7**, 7-11 (2006)
2. M. V. Borunov, P. N. Nadtochy, G. D. Adeev, *Nucl. Phys*. **A**, doi:10.1016/j.nuclphysa.2007.11.002
3. H. Goutte, J. F. Berger, P. Casoli, D. Gogny, *Phys. Rev.* **C 71,** 024316 (2005)
4. S. Borzakov, A. Andreev, E. Dermendjiev, A. Filip, W. Furman, Ts. Panteleev, I. Ruskov, Yu. Zamyatnin, Sh. Zeinalov, *Phys. At. Nuclei* **63,** 530-538 (2000)
5. S. G. Prussin, M.-A. Descalle, J. M. Hall, J. A. Pruet, D. R. Slaughter, M. R. Accatino, O. J. Alford, S. J. Asztalos, A. Bernstein, J. A. Church, *Nucl. Instrum. Methods* **A 569**, 853-862 (2007)
6. FAIR: http://www.gsi.de/fair
7. EURISOL: http://www.eurisol.org
8. A. G. W. Cameron, *The Astroph. J.* **587**, 327 (2003)
9. K.-H. Schmidt, S. Steinhäuser, C. Böckstiegel, A. Grewe, A. Heinz, A. R. Junghans, J. Benlliure, H.-G. Clerc, M. de Jong, J. Müller, M. Pfützner, B. Voss, *Nucl. Phys.* **A 665**, 221-267 (2000)
10. K.-H. Schmidt, J. Benlliure, A. R. Junghans, *Nucl. Phys.* **A 693**, 169-189 (2001)
11. V. V. Pashkevich, *Nucl. Phys.* **A 169**, 275-293 (1971)
12. U. Brosa, S. Grossmann, A. Müller, *Phys. Rep.* **197**, 167-262 (1990)
13. B. D. Wilkins, E. P. Steinberg, R. R: Chasman, *Phys. Rev.* **C 14**, 1832-1863 (1976)
14. C. Böckstiegel, S. Steinhäuser, K.-H. Schmidt, H.-G. Clerc, A. Grewe, A. Heinz, M. de Jong, A. R. Junghans, J. Müller, B. Voss, *arXiv: nucl-ex*/0712.3808 and to be published
15. J. P. Unik, J. E. Gindler, L. E. Glendenin, K. F. Flynn, A. Gorski, R. K. Sjoblom, *Proc. Symp. on Physics and Chem. in Fission*, Rochester 1973, IAEA Vienna 1974, Vol. 2, p. 19
16. R. Vandenbosch, J. R. Huizenga, *Nuclear Fission* (New York: Academic), 1993
17. A. V. Karpov, R. M. Hiryanov, A. V. Sagdeev , G. D. Adeev, *J. Phys. G: Nucl. Part. Phys.* **34**, 255-269 (2007)
18. G. D. Adeev, V. V. Pashkevich, *Nucl. Phys.* **A 502**, 405c-422c (1989)
19. A. V. Karpov, G. D. Adeev, *Eur. Phys. J.* **A 14**, 169-178 (2002)
20. S. I. Mulgin, K.-H. Schmidt, A. Grewe, S. V. Zhdanov, *Nucl. Phys.* **A 640**, 375-388 (1998)
21. M. G. Itkis, S. I.Mulgin, A. Ya, Rusanov et al., *Sov. J. Nucl. Phys*. **34**, 719 (1986)
22. A. Ya, Rusanov, M. G. Itkis, V. N. Okolovich, *Phys. Atom. Nucl.* **60**, 683-712 (1997)
23. K.-H. Schmidt, A. Kelić, M. V. Ricciardi, *arXiv: nucl-ex*/0711.3967 and to be published
24. U. Mosel, H. W. Schmitt, *Nucl. Phys.* **A 165**, 73-96 (1971)
25. I. Ragnarsson, R. K. Sheline, *Phys. Scr.* **29**, 385-401 (1984)
26. P. Möller, D. G. Madland, A. J. Sierk, A. Iwamoto, *Nature* **409**, 785-790 (2001)